The 2010 IEEE/RSJ International Conference on
Intelligent Robots and Systems
October 18-22, 2010, Taipei, Taiwan

High-speed Biped Gait Generation Based on Asymmetrization of Impact Posture Using Telescopic Legs

Fumihiko Asano

Abstract— **The author has proposed a novel method for generating a dynamic gait based on anterior-posterior asymmetric impact posture tilting the robot's center of mass forward. The primary purpose of this method is to asymmetrize the impact posture by actuating the robot's telescopic-legs to make overcoming the potential barrier at mid-stance easy, and the mechanical energy is accordingly restored. We have already validated our method through numerical investigations of a planar rimless wheel model with telescopic legs. The results implied that the robot motion becomes remarkably high-speed and the need of ankle brake was indicated. This paper then extends the method to a planar telescopic-legged biped model incorporating the brake effect of ankle spring, and numerically investigate the gait properties. We also discuss the role of anterior-posterior asymmetric shape of human foot from the viewpoint of zero moment point.**

I. INTRODUCTION

Limit cycle walkers can generate natural and energy-efficient dynamic gaits utilizing their own physical dynamics and passivity. By applying a suitable actuation rule to the robot, efficient level walking can be achieved [1][2][3][4][5], however, guaranteeing the limit cycle stability is another problem and is not easy.

One of the most impeditive problems in stable limit cycle generation is the potential barrier at mid-stance. The robot must start walking with a suitable and sufficient initial momentum to overcome the potential barrier and to reach the next impact. It is not easy to guarantee overcoming the potential barrier only with intuitive control laws in limit cycle walking. It is also difficult to start walking from a standing posture smoothly and we must search the suitable initial conditions through a trial and error process.

The potential barrier in dynamic gait originally comes from the fact that limit cycle walkers have anterior-posterior symmetric impact posture as shown in Fig. 1 (a). To solve this problem, the author proposed a method for generating a gait that guarantees to overcome the potential barrier by asymmetrizing the impact posture as shown in Fig. 1 (b). The primary purpose of this method is to tilt or shift the robot's center of mass (CoM) forward for overcoming the potential barrier at mid-stance easily. The easiest way to asymmetrize the impact posture is to extend the stance leg during stance phases using the prismatic joints or knee joints. The author numerically investigated the validity of the proposed method using a telescopic-legged rimless wheel model shown in Fig. 2 (a), and performed parameter study in [6]. We showed the possibility of stable gait generation on level ground using the model, and extended it to climbing up a steep slope as shown in Fig. 2 (b). The simulation results implied that the generated level gaits are remarkably high-speed and the robot would jump because of the overly rapid motion. Through our investigations, the need of ankle brake has been indicated. The importance of forward-bending impact posture has been also discussed in several related works [2][3][4].

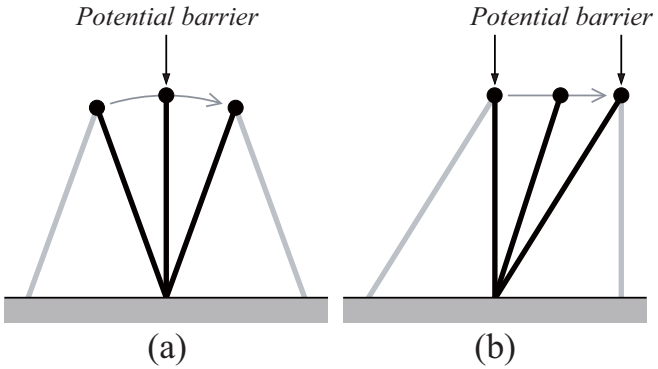

Fig. 1. Relations between impact posture and potential barrier

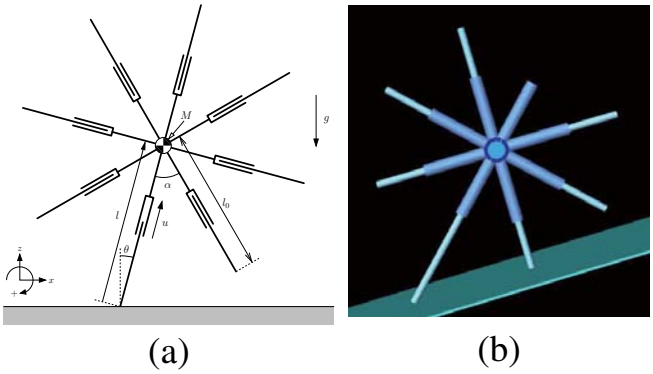

Fig. 2. Telescopic-legged rimless wheel that can climb up slopes

On the other hand, the author has wondered about the meaning of anterior-posterior asymmetry of human foot. As the authors have shown, such as in virtual passive dynamic walking, the stance leg of limit cycle walkers must be driven forward during stance phases to generate an energy-efficient level gait without creating negative input power [5][7]. The zero moment point (ZMP) is then shifted posterior to the ankle joint. This implies that the heel-side must be longer than toe-side in robot foot. Human foot is, however, formed of inverse shape and this implies that it can drive the stance leg backward only. In other words, human foot is not suitable to drive the body forward.

Based on the observations, in this paper, we extend our

F. Asano is with the School of Information Science, Japan Advanced Institute of Science and Technology, 923-1292 Ishikawa, Japan fasano@jaist.ac.jp

gait generation method to a planar telescopic-legged biped robot with feet incorporating a brake spring and numerically investigate the gait descriptors, especially the behavior of ZMP. Through numerical simulations, we discuss the anterior-posterior asymmetry of human foot from the ZMP point of view.

II. MODELING OF TELESCOPIC-LEGGED BIPED

A. Modeling of Biped Robot

1) Dynamic equation: Fig. 3 shows the planar telescopic-legged biped model. Let the stance leg and swing leg be Leg 1 and Leg 2, and $\boldsymbol{q}_i = \left[\begin{array}{cccc} x_i & z_i & \theta_i & b_i \end{array}\right]^{\mathrm{T}}$ be the generalized coordinate vector for Leg i. The corresponding dynamic equation becomes

$$\boldsymbol{M}_i(\boldsymbol{q}_i)\ddot{\boldsymbol{q}}_i + \boldsymbol{h}_i(\boldsymbol{q}_i, \dot{\boldsymbol{q}}_i) = \boldsymbol{0}_{4\times 1}, \tag{1}$$

and we then augment them by adding the holonomic constraint forces and control inputs. The two legs are connected at the hip joint. We also assume that the foot mass and thin are ignorable or the foot dynamics does not affect the walking motion at all. Let $\boldsymbol{q} = \left[\begin{array}{cc} \boldsymbol{q}_1^{\mathrm{T}} & \boldsymbol{q}_2^{\mathrm{T}} \end{array}\right]^{\mathrm{T}}$ be the generalized coordinate vector of the whole walking system, the dynamic equation then becomes

$$\boldsymbol{M}(\boldsymbol{q})\ddot{\boldsymbol{q}} + \boldsymbol{h}(\boldsymbol{q}, \dot{\boldsymbol{q}}) = \boldsymbol{S}\boldsymbol{u} + \boldsymbol{J}(\boldsymbol{q})^{\mathrm{T}}\boldsymbol{\lambda}, \quad \boldsymbol{J}(\boldsymbol{q})\dot{\boldsymbol{q}} = \boldsymbol{0}_{4\times 1}, \tag{2}$$

where $\boldsymbol{S}\boldsymbol{u} \in \mathbb{R}^8$ is the control input vector, $\boldsymbol{J}(\boldsymbol{q})^{\mathrm{T}}\boldsymbol{\lambda} \in \mathbb{R}^8$ is the holonomic constraint force vector for connecting the two legs. The terms in Eq. (2) are detailed as

$$\boldsymbol{M}(\boldsymbol{q}) = \left[\begin{array}{cc} \boldsymbol{M}_1(\boldsymbol{q}_1) & \boldsymbol{0}_{4\times 4} \\ \boldsymbol{0}_{4\times 4} & \boldsymbol{M}_2(\boldsymbol{q}_2) \end{array}\right], \tag{3}$$

$$\boldsymbol{h}(\boldsymbol{q}, \dot{\boldsymbol{q}}) = \left[\begin{array}{c} \boldsymbol{h}_1(\boldsymbol{q}_1, \dot{\boldsymbol{q}}_1) \\ \boldsymbol{h}_2(\boldsymbol{q}_2, \dot{\boldsymbol{q}}_2) \end{array}\right]. \tag{4}$$

By eliminating $\boldsymbol{\lambda}$ from Eq. (2), the dynamic equation is arranged as

$$\begin{aligned} \boldsymbol{M}(\boldsymbol{q})\ddot{\boldsymbol{q}} &= \boldsymbol{Y}(\boldsymbol{q})\left(\boldsymbol{S}\boldsymbol{u} - \boldsymbol{h}(\boldsymbol{q}, \dot{\boldsymbol{q}})\right) \\ &\quad -\boldsymbol{J}(\boldsymbol{q})^{\mathrm{T}}\boldsymbol{X}(\boldsymbol{q})^{-1}\dot{\boldsymbol{J}}(\boldsymbol{q}, \dot{\boldsymbol{q}})\dot{\boldsymbol{q}}, \qquad (5) \\ \boldsymbol{Y}(\boldsymbol{q}) &= \boldsymbol{I}_8 - \boldsymbol{J}(\boldsymbol{q})^{\mathrm{T}}\boldsymbol{X}(\boldsymbol{q})^{-1}\boldsymbol{J}(\boldsymbol{q})\boldsymbol{M}(\boldsymbol{q})^{-1}, \qquad (6) \\ \boldsymbol{X}(\boldsymbol{q}) &= \boldsymbol{J}(\boldsymbol{q})\boldsymbol{M}(\boldsymbol{q})^{-1}\boldsymbol{J}(\boldsymbol{q})^{\mathrm{T}}. \qquad (7) \end{aligned}$$

The control input vector is also detailed as

$$\boldsymbol{S}\boldsymbol{u} = \left[\begin{array}{ccc} 0 & 0 & 0 \\ 0 & 0 & 0 \\ 0 & 0 & 1 \\ 1 & 0 & 0 \\ 0 & 0 & 0 \\ 0 & 0 & 0 \\ 0 & 0 & -1 \\ 0 & 1 & 0 \end{array}\right] \left[\begin{array}{c} u_1 \\ u_2 \\ u_H \end{array}\right]. \tag{8}$$

The ankle-joint torque, u_A, is added later.

2) Transition equations: The positions are exchanged in accordance with the geometrical conditions as follows:

$$\begin{aligned} x_1^+ &= 0, \quad z_1^+ = 0, \quad \theta_1^+ = \theta_2^-, \quad \theta_2^+ = \theta_1^-, \qquad (9) \\ x_2^+ &= x_1^+ + l_1\sin\theta_1^+ - l_2\sin\theta_2^+ = -x_2^-, \qquad (10) \\ z_2^+ &= z_1^+ + l_1\cos\theta_1^+ - l_2\cos\theta_2^+ = -z_2^- = 0. \qquad (11) \end{aligned}$$

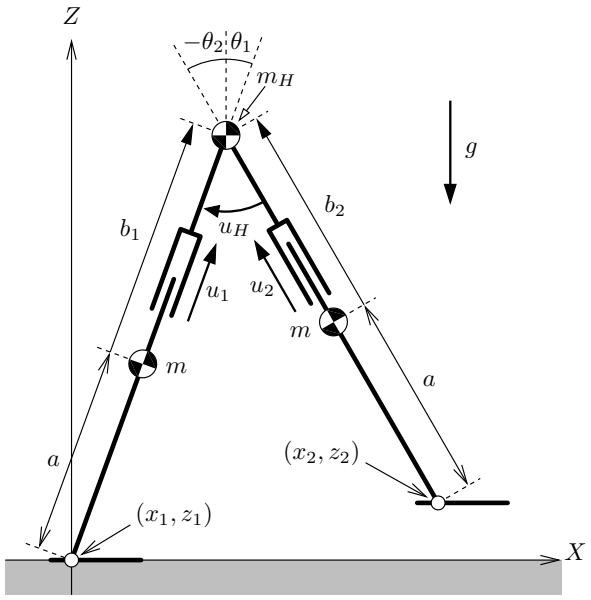

Fig. 3. Model of planar telescopic-legged biped robot with feet

Next, the transition equations for the velocities are described. We first calculate the velocities just after impact without switching the legs. After that, we exchange the velocities of Leg 1 for those of Leg 2. Assuming that Leg 1 leaves the floor just after impact, the inelastic collision is modeled as

$$\begin{aligned} \boldsymbol{M}(\boldsymbol{q})\dot{\boldsymbol{q}}^+ &= \boldsymbol{M}(\boldsymbol{q})\dot{\boldsymbol{q}}^- - \boldsymbol{J}_I(\boldsymbol{q})^{\mathrm{T}}\boldsymbol{\lambda}_I, \qquad (12) \\ \boldsymbol{J}_I(\boldsymbol{q})\dot{\boldsymbol{q}}^+ &= \boldsymbol{0}_{7\times 1}. \qquad (13) \end{aligned}$$

The Jacobian matrix $\boldsymbol{J}_I(\boldsymbol{q})$ is derived as follows. The conditions that the tip of Leg 2 is fixed on the floor without slipping just after impact are given by

$$\dot{x}_2^+ = 0, \quad \dot{z}_2^+ = 0. \tag{14}$$

We also assume that the prismatic joints of the legs are mechanically locked at impact, and the conditions are given by

$$\dot{b}_1^+ = 0, \quad \dot{b}_2^+ = 0. \tag{15}$$

Following these conditions, the lengths of both legs, $l_1 := a + b_1$ and $l_2 := a + b_2$, are treated as constants at impact. In addition, the conditions that the hip positions of both legs are identical are given by

$$\begin{aligned} \frac{\mathrm{d}}{\mathrm{d}t}\left(x_1 + l_1\sin\theta_1\right)^+ &= \frac{\mathrm{d}}{\mathrm{d}t}\left(x_2 + l_2\sin\theta_2\right)^+, \qquad (16) \\ \frac{\mathrm{d}}{\mathrm{d}t}\left(z_1 + l_1\cos\theta_1\right)^+ &= \frac{\mathrm{d}}{\mathrm{d}t}\left(z_2 + l_2\cos\theta_2\right)^+, \qquad (17) \end{aligned}$$

and these lead to

$$\begin{aligned} \dot{x}_1^+ + l_1\dot{\theta}_1^+\cos\theta_1 &= \dot{x}_2^+ + l_2\dot{\theta}_2^+\cos\theta_2, \qquad (18) \\ \dot{z}_1^+ - l_1\dot{\theta}_1^+\sin\theta_1 &= \dot{z}_2^+ - l_2\dot{\theta}_2^+\sin\theta_2. \qquad (19) \end{aligned}$$

To cancel out the tracking error, we further consider another condition that the relative hip-joint, $\theta_H := \theta_1 - \theta_2$ is mechanically locked at impact:

$$\dot{\theta}_H^+ = 0. \tag{20}$$

Following the above conditions, we can precisely achieve $\boldsymbol{y} \equiv \boldsymbol{y}_{\rm d}$ without PD feedback because all velocities of the output just after impact, $\dot{\boldsymbol{y}}^+$, become zero. The control input can be specified only by feed-forward of the desired acceleration, and we can examine the gait efficiency reflecting the desired trajectories accurately.

Summarizing the above seven velocity constraint conditions of (14), (15), (18), (19) and (20), matrix $\boldsymbol{J}_I(\boldsymbol{q}) \in \mathbb{R}^{7\times 8}$ is specified as follows:

$$\boldsymbol{J}_I(\boldsymbol{q}) = \begin{bmatrix} 1 & 0 & J_{13} & J_{14} & -1 & 0 & J_{17} & J_{18} \\ 0 & 1 & J_{23} & J_{24} & 0 & -1 & J_{27} & J_{28} \\ 0 & 0 & 0 & 0 & 1 & 0 & 0 & 0 \\ 0 & 0 & 0 & 0 & 0 & 1 & 0 & 0 \\ 0 & 0 & 0 & 1 & 0 & 0 & 0 & 0 \\ 0 & 0 & 0 & 0 & 0 & 0 & 0 & 1 \\ 0 & 0 & 1 & 0 & 0 & 0 & -1 & 0 \end{bmatrix}, \quad (21)$$

where

$$\begin{aligned} &J_{13} = l_1 \cos\theta_1, \quad J_{14} = \sin\theta_1, \quad J_{17} = -l_2 \cos\theta_2, \\ &J_{18} = -\sin\theta_2, \quad J_{23} = -l_1 \sin\theta_1, \quad J_{24} = \cos\theta_1, \\ &J_{27} = l_2 \sin\theta_2, \quad J_{28} = -\cos\theta_2. \end{aligned}$$

Matrix $\boldsymbol{J}(\boldsymbol{q})$ in Eq. (2) is also derived as

$$\boldsymbol{J}(\boldsymbol{q}) = \begin{bmatrix} 1 & 0 & J_{13} & J_{14} & -1 & 0 & J_{17} & J_{18} \\ 0 & 1 & J_{23} & J_{24} & 0 & -1 & J_{27} & J_{28} \\ 1 & 0 & 0 & 0 & 0 & 0 & 0 & 0 \\ 0 & 1 & 0 & 0 & 0 & 0 & 0 & 0 \end{bmatrix}. \quad (22)$$

We can finally accomplish the transition by replacing $\dot{\boldsymbol{q}}_1^+$ with $\dot{\boldsymbol{q}}_2^+$ in $\dot{\boldsymbol{q}}^+ = \left[\begin{array}{cc} \dot{\boldsymbol{q}}_1^+ & \dot{\boldsymbol{q}}_2^+ \end{array}\right]^{\rm T}$.

B. Control laws

We choose the two telescopic-leg lengths and the relative hip angle as the control output. The output vector, $\boldsymbol{y} \in \mathbb{R}^3$, is then defined as

$$\boldsymbol{y} = \begin{bmatrix} b_1 \\ b_2 \\ \theta_H \end{bmatrix} = \boldsymbol{S}^{\rm T}\boldsymbol{q}, \quad (23)$$

and its second-order derivative with respect to time becomes

$$\ddot{\boldsymbol{y}} = \boldsymbol{S}^{\rm T}\ddot{\boldsymbol{q}} = \boldsymbol{A}(\boldsymbol{q})\boldsymbol{u} + \boldsymbol{B}(\boldsymbol{q}, \dot{\boldsymbol{q}}), \quad (24)$$

where

$$\begin{aligned} \boldsymbol{A}(\boldsymbol{q}) &= \boldsymbol{S}\left(\boldsymbol{I}_8 - \boldsymbol{M}(\boldsymbol{q})^{-1}\boldsymbol{J}(\boldsymbol{q})^{\rm T}\boldsymbol{X}(\boldsymbol{q})^{-1}\boldsymbol{J}(\boldsymbol{q})\right) \\ &\quad \times \boldsymbol{M}(\boldsymbol{q})^{-1}\boldsymbol{S}, \quad (25) \\ \boldsymbol{B}(\boldsymbol{q}, \dot{\boldsymbol{q}}) &= -\boldsymbol{S}^{\rm T}\boldsymbol{M}(\boldsymbol{q})^{-1}\boldsymbol{h}(\boldsymbol{q}, \dot{\boldsymbol{q}}) + \boldsymbol{S}^{\rm T}\boldsymbol{M}(\boldsymbol{q})^{-1}\boldsymbol{J}(\boldsymbol{q})^{\rm T} \\ &\quad \times \boldsymbol{X}(\boldsymbol{q})^{-1}\left(\boldsymbol{J}(\boldsymbol{q})\boldsymbol{M}(\boldsymbol{q})^{-1}\boldsymbol{h}(\boldsymbol{q}, \dot{\boldsymbol{q}}) - \dot{\boldsymbol{J}}(\boldsymbol{q}, \dot{\boldsymbol{q}})\dot{\boldsymbol{q}}\right). \quad (26) \end{aligned}$$

Then we can consider the following control input for achieving $\boldsymbol{y} \to \boldsymbol{y}_{\rm d}$.

$$\begin{aligned} \boldsymbol{u} &= \boldsymbol{A}(\boldsymbol{q})^{-1}\left(\boldsymbol{v} - \boldsymbol{B}(\boldsymbol{q}, \dot{\boldsymbol{q}})\right) \quad (27) \\ \boldsymbol{v} &= \ddot{\boldsymbol{y}}_{\rm d} + \boldsymbol{K}_{\rm D}\left(\dot{\boldsymbol{y}}_{\rm d} - \dot{\boldsymbol{y}}\right) + \boldsymbol{K}_{\rm P}\left(\boldsymbol{y}_{\rm d} - \boldsymbol{y}\right) \quad (28) \end{aligned}$$

By adding the condition of Eq. (20), all elements of $\dot{\boldsymbol{y}}^+$ become zero and the trajectory tracking control without any tracking errors, $\boldsymbol{y} \equiv \boldsymbol{y}_{\rm d}(t)$, is achieved only by the feed-forward control of the desired accelerations.

The time-dependent desired trajectories, $\boldsymbol{y}_{\rm d}(t)$, are specified as 5-order functions for smoothly interporating between the boundary conditions, and all the outputs are smoothly controlled from the initial conditions to the final ones in each step.

III. NUMERICAL ANALYSES

A. Starting from Standing Posture

We first consider a starting control and stable gait generation from a static standing posture. The robot starts walking from a standing posture ($b_1 = b_2 = b$, $\theta_1 = \theta_2 = 0$) and static condition ($\dot{\theta}_1 = \dot{\theta}_2 = 0$, $\dot{b}_1 = \dot{b}_2 = 0$), and generate the dynamic gait while updating the desired trajectories in accordance with the following strategy.

The telescopic-leg length of the stance leg, b_1, is controlled to follow its desired time-dependent trajectory, $b_{1\rm d}(t)$, from the length just after impact, b_1^+, to the terminal value, $b+\Delta b$. We consider a time-dependent 5-order function to smoothly interpolate the values, and update the coefficients at every impact. The telescopic-leg length of the swing leg, b_2, and the relative hip angle, θ_H, are also controlled to follow their desired trajectories, $b_{2\rm d}(t)$ and $\theta_{H\rm d}(t)$, in the same manner as b_1. This will result in that, after the second impact, b_1 is controlled from $b - \Delta b$ to $b + \Delta b$, b_2 is controlled from $b + \Delta b$ to $b - \Delta b$, and θ_H is controlled from $-\alpha$ to α by following their smooth desired trajectories. The telescopic-legged rimless wheel must start with a small initial velocity to fall down [6], whereas a biped robot can start the walking from a static standing posture only by creating the first impact posture because this results in shifting the CoM forward.

Fig. 4 shows the simulation results of dynamic walking from a static standing posture where $\Delta b = 0.05$ [m]. We can see that a stable 1-period gait is generated. Fig. 5 shows the stick diagram for one cycle. The system parameters were chosen as listed in Table I. The desired settling time for shortening the swing-leg length, $T_{\rm set}^2$, were chosen as a shorter value than others to guarantee the foot clearance.

The most remarkable result is the high walking speed. In this case, the walking speed converged to 1.31 [m/s]. It is reported that the average walking speed of adult humans is 82 [m/min] (= 1.367 [m/s]) in [8]. We can find that the walking speed of the generated gait approaches to that of humans. Compared to the results of virtual passive dynamic walking and energy tracking control [5][7], the obtained walking speed is found to be remarkably fast. Although we cannot avoid the deterioration of energy-efficiency, the proposed approach enables the robot to generate a remarkably high-speed gait that the previous methods could not achieve. Note also that the gait generation does not depend on the effect of semicircular feet [9][10].

From Fig. 4(d), we can see that sufficiently large ground reaction force is generated during stance phases compared to the case of the telescopic-legged rimless wheel. This is because the lower part of the leg is heavy.

From Fig. 4(e), we can see that negative input power occurs during posterior half of cycle. This is caused by the

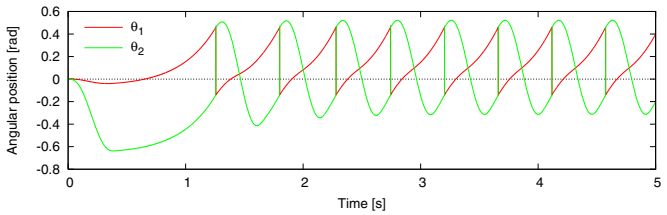

(a) Angular position

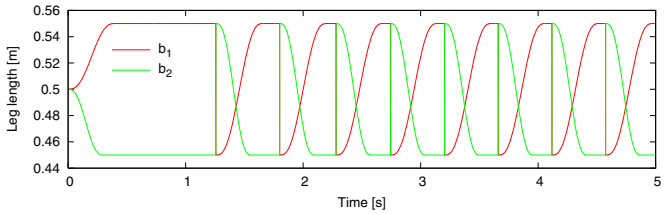

(b) Telescopic-leg length

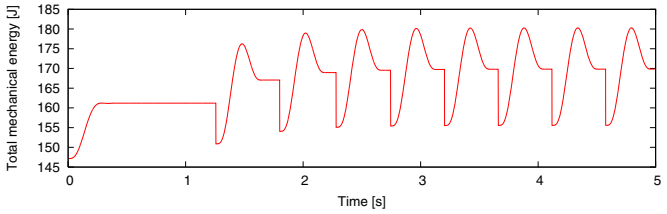

(c) X-position of CoM

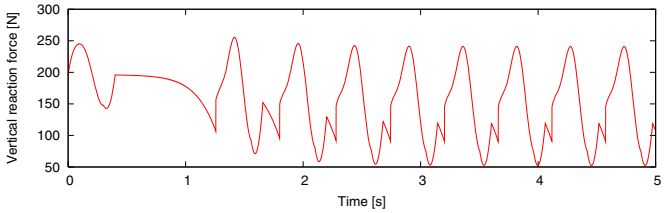

(d) Vertical reaction force

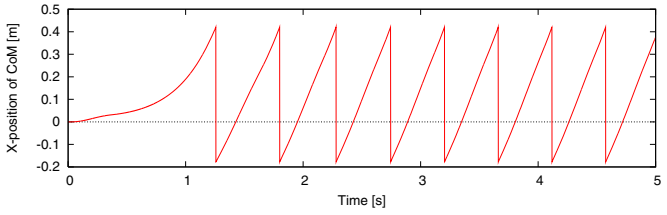

(e) Total mechanical energy

Fig. 4. Simulation results of dynamic walking from standing posture where $\Delta b = 0.05$ [m]

tracking control to the time-dependent desired trajectories. As mentioned later, the gait generation becomes impossible as Δb decreases more. In this case, the robot must utilize the ankle-joint actuation or it cannot obtain sufficient driving force to overcome the potential barrier.

B. Efficiency Analysis Considering Ankle-joint Torque

In the case of the telescopic-legged rimless wheel, remarkably high-speed level gaits near-running were generated [6]. In return for it, however, the motion was too rapid to satisfy the desired settling-time condition for the telescopic-leg actuation. As a candidate of the solution to this problem, a brake effect by the ankle-joint actuation can be considered. By driving the stance leg backward, we can extend the time margin, i.e., the step period.

TABLE I

PHYSICAL AND CONTROL PARAMETERS OF BIPED WALKING SYSTEM

m_H	10.0	kg	α	0.60	rad
m	5.0	kg	$T_{\rm set}^1$	0.40	s
a	0.50	m	$T_{\rm set}^2$	0.30	s
b	0.50	m	$T_{\rm set}^H$	0.40	s

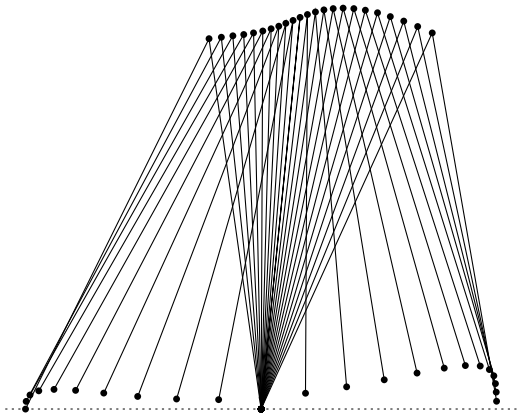

Fig. 5. Stick diagram for steady gait where $\Delta b = 0.05$ [m]

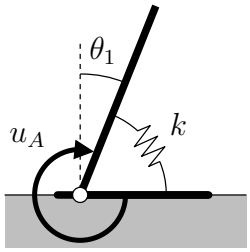

Fig. 6. Foot mechanism with elastic element

In this section, we consider the foot mechanism with an elastic element as shown in Fig. 6, and apply its effect as the ankle-joint torque to the robot. We assume that the elastic element becomes natural length when $\theta_1 = 0$, and the ankle-joint torque, u_A, is then given by

$$u_A = -k\theta_1, \tag{29}$$

where k [N·m] is a positive constant which stands for the elastic coefficient. The ankle-joint torque vector then becomes

$$\boldsymbol{S}_A u_A = \begin{bmatrix} 0 & 0 & 1 & 0 & 0 & 0 & 0 & 0 \end{bmatrix}^{\rm T} u_A, \tag{30}$$

and we add this to the right-hand side of Eq. (2) to calculate $\boldsymbol{\lambda}$. Also note that $\boldsymbol{h}(\boldsymbol{q}, \dot{\boldsymbol{q}})$ in Eq. (26) must be replaced with $\boldsymbol{h}(\boldsymbol{q}, \dot{\boldsymbol{q}}) - \boldsymbol{S}_A u_A$ to calculate $\boldsymbol{B}(\boldsymbol{q}, \dot{\boldsymbol{q}})$.

Fig. 7 shows the gait descriptors with respect to Δb changing it by 0.005 [m]. We plotted the results, however, only in the case the generated gait was 1-period stable. The elastic coefficient, k, was chosen as 0.0, 5.0, 10.0, 15.0 and 20.0 [N·m].

From Fig. 7(a), we can see that the step period monotonically decreases with the increase of Δb in all cases. In addition, enough settling-time margin is created when k

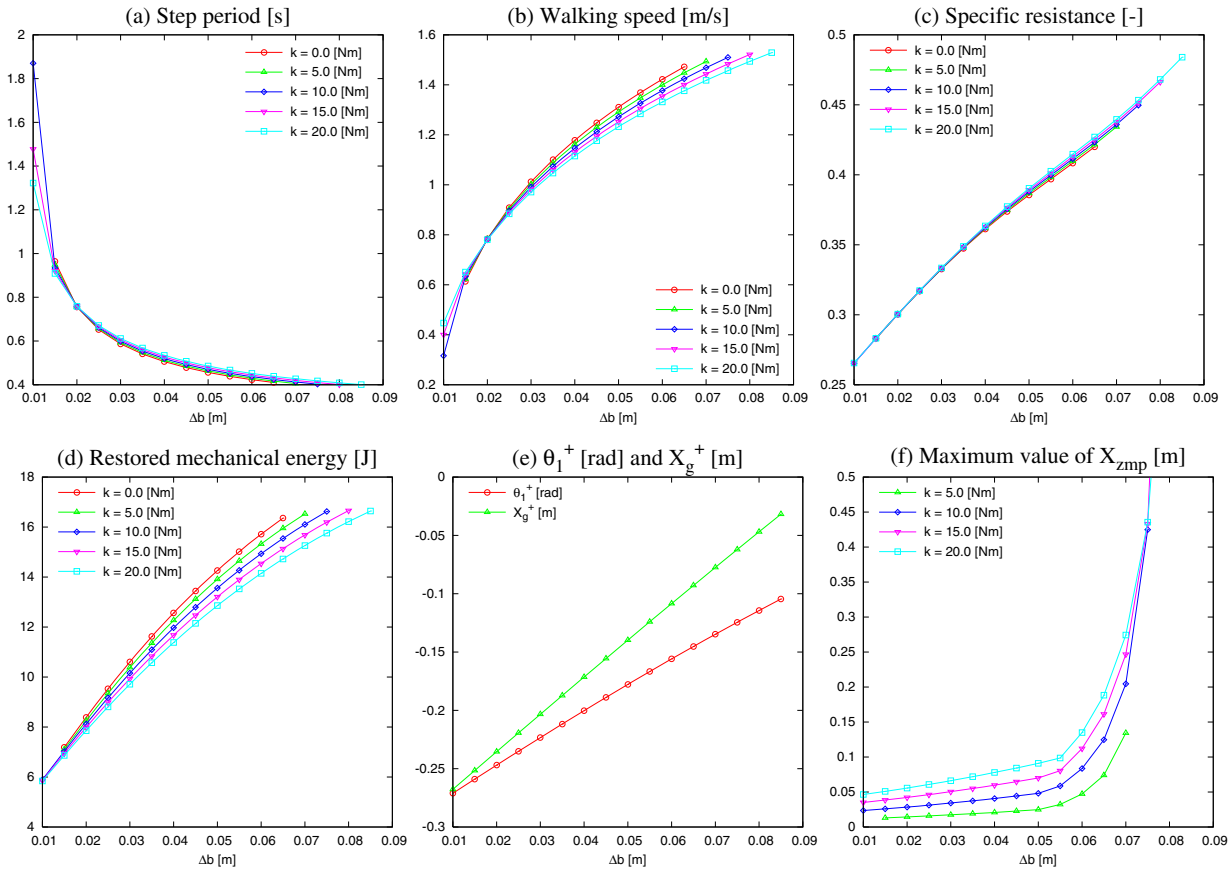

Fig. 7. Gait descriptors with respect to Δb for five values of k

is large. The maximum desired settling time is chosen as $T^1_{\rm set} = T^H_{\rm set} = 0.40$ [s], and the step period must be longer than it. In all cases, this condition becomes impossible to be met as the impact posture is asymmetrized. When Δb is large, the larger k becomes, the longer the settling-time margin becomes by the brake effect of u_A. When Δb is small ($\Delta b \leq 0.02$ [m]), however, this tendency reverses. In addition, stable gaits are generated even if $\Delta b = 0.01$ [m] where $k = 10.0$, 15.0, and 20.0. This is because u_A becomes positive during the first phase of cycle or when θ_1 is negative and it helps to overcome the potential barrier.

From Fig. 7(b), we can see that the walking speed monotonically increases with the increase of Δb in all cases. The step length is identical to the horizontal distance the robot travels, ΔX_g [m], and it satisfies

$$\Delta X_g^2 = (a+b+\Delta b)^2 + (a+b-\Delta b)^2 - 2(a+b+\Delta b)(a+b-\Delta b)\cos\alpha, \quad (31)$$

$$\frac{\partial \Delta X_g^2}{\partial \Delta b} = 4\,(1+\cos\alpha)\,\Delta b. \quad (32)$$

Then we can find that it monotonically increases with respect to Δb. Since the walking speed is calculated as $\Delta X_g/T$ [m/s], we can conclude that the walking speed increases by the synergistic effect of the increment of ΔX_g and the decrement of step period. The increasing tendency of ΔX_g is less than that of Δb, however, the walking speed fundamentally changes inversely proportional to the step period.

From Fig. 7(c), we can see that the specific resistance (SR) monotonically increases with the increase of Δb in all cases. It is natural that the consumed energy increases with respect to the leg extension and its control speed, and this result implies that the increasing tendency of the consumed energy (average input power) is more than that of the walking speed. As a candidate of solution to improve the energy-efficiency, extension of the desired settling-time in accordance with the step period extended by the brake effect of u_A. We would like to leave the detailed analysis for another opportunity.

Note that we did not take u_A into account to calculate the SR because it is not an input torque but an elastic force. The average input power is thus defined as

$$p = \frac{1}{T}\int_{0^+}^{T^-} \left(\left|\dot{b}_1 u_1\right| + \left|\dot{b}_2 u_2\right| + \left|\dot{\theta}_H u_H\right|\right) \mathrm{d}t. \quad (33)$$

Fig. 7(e) plots θ_1 and X_g just after impact. We plotted the analysis results where $k = 20.0$ only because the impact posture is uniquely determined according to Δb regardless of k. In all cases, the values of X_g^+ are negative, that is, the generated impact postures cannot guarantee to overcome the potential barrier. Also the values of θ_1^+ are always negative. This implies that the hip position does not shift anterior to the forefoot point at impact. Let's consider these results from

the angular momentum point of view. Let L [kg·m^2/s] be the angular momentum around the foot point, its time-derivative then satisfies

$$\dot{L} = u_A + MgX_g, \tag{34}$$

where M [kg] is the robot's total mass. The angular momentum draws a curve convex downward with respect to time in the presence of potential barrier [11]. If the robot achieves the sufficient condition for overcoming the potential barrier, $X_g^+ \geq 0$, however, $\dot{L}$ becomes always positive and L then monotonically increases. The analysis results imply that a dynamic gait achieving $X_g^+ \geq 0$ or $\dot{L} \geq 0$ is extremely high-speed and is hard to be realized. In other words, achieving $X_g^+ < 0$ or creating the phase with $\dot{L} < 0$ prevents the excessive forward acceleration for generating a stable gait.

Let R_Z [N] be the vertical ground reaction force, then the X-position of ZMP of the biped model is given by

$$X_{\rm zmp} = \frac{k\theta_1}{R_Z}. \tag{35}$$

Fig. 7(f) plots its maximum values. We omitted the result where $k = 0.0$ [N·m] because the value is always kept zero. We can see that the values monotonically increase with respect to Δb and there is a significant change in the increasing tendency of the maximum ZMP around $\Delta b = 0.055$ [m] in all cases. Fig. 8 shows the steady ZMP pattern with respect to time for two Δb where $k = 20.0$. In the case of $\Delta b = 0.040$ [m], there is a change or indifferentiable point in the ZMP motion just prior to impact. This is because the telescopic-leg actuation is completed at this instant (the desired settling time, $t = T_{\rm set1}$), and the robot begins to fall down as a 1-dof rigid body. As a result, the peak just prior to the settling time yields the maximum value of ZMP. Whereas in the case of $\Delta b = 0.070$ [m], there is little time-margin and the heel-strike occurs just after the settling time, and the peak during the control phases yields the maximum ZMP. In each case, the properties that the ZMP moves from heel to toe, and that the ZMP remains within the area anterior to the ankle joint during most part of cycle are the same and are similar to human walking.

In addition, note that the forefoot must be longer than 30 [cm] where $k = 20.0$ [N·m] as shown in Fig. 7 (f). In humans, as shown in Fig. 9, the heel would rise up or the motion of forefoot weight-bearing [8] would start in this

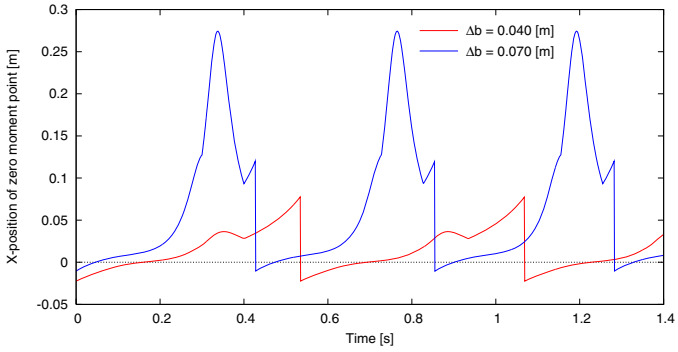

Fig. 8. Time evolutions of $X_{\rm zmp}$ for two values of Δb

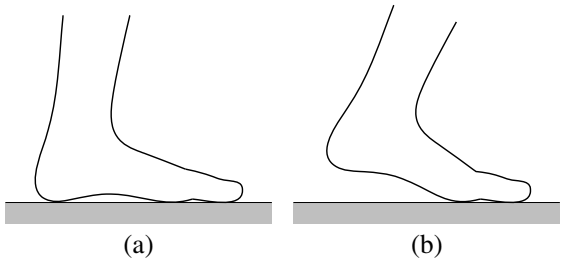

Fig. 9. Foot flat weight-bearing (a) and forefoot weight-bearing (b)

case. In the future, we should investigate the gait properties and perform numerical simulations taking forefoot weight-bearing in to account.

IV. CONCLUSION AND FUTURE WORK

In this paper, we have extended the gait generation method based on asymmetric impact posture to a planar telescopic-legged biped with feet, and conducted parameter study taking the ankle-joint actuation into account. We also discussed the role of asymmetric shape of human foot from the viewpoint of the ankle brake effect. The simulation results showed that the ankle-joint torque as a brake is effective to generate a stable gait in terms of extending the time margin, and the toe-side must be longer than heel-side to cover the ZMP.

Another way to create an impact posture tilting forward is bending the knee joints. Now we are examining the effect using various walking models and the results will be reported in our future paper. Utilizing the upper body is also an interesting approach and is left as a future work.

REFERENCES

[1] S. Collins, A. Ruina, R. Tedrake and M. Wisse, "Efficient bipedal robots based on passive-dynamic walkers," *Science*, Vol. 307, No. 5712, pp. 1082–1085, 2005.

[2] J. Zhang, M. Zhao and H. Dong, "Effect of energy feedbacks on virtual slope walking: I. Complementary energy feedback," *Proc. of the IEEE Int. Conf. on Robotics and Automation*, pp. 1959–1965, 2009.

[3] T. Hayashi, F. Asano, Z.W. Luo, A. Nagano, K. Kaneko and A. Kato, "Experimental study of a parametrically excited dynamic bipedal walker with counterweights," *Proc. of the IEEE/RSJ Int. Conf. on Intelligent Robots and Systems*, pp. 81–86, 2009.

[4] Y. Harata, F. Asano, K. Taji and Y. Uno, "Parametric excitation walking for four-linked bipedal robot," *Proc. of the 9th Int. IFAC Symp. on Robot Control*, pp. 589–594, 2009.

[5] F. Asano, Z.W. Luo and M. Yamakita, "Biped gait generation and control based on a unified property of passive dynamic walking," *IEEE Trans. on Robotics*, Vol. 21, No. 4, pp. 754–762, 2005.

[6] F. Asano, "Dynamic gait generation of telescopic-legged rimless wheel based on asymmetric impact posture," *Proc. of the 9th IEEE-RAS Int. Conf. on Humanoid Robots*, pp. 68–73, 2009.

[7] F. Asano and Z.W. Luo, "Asymptotically stable biped gait generation based on stability principle of rimless wheel," *Robotica*, Vol. 27, No. 6, pp. 949–958, 2009.

[8] J. Perry, Gait analysis: Normal and pathological function, SLACK Inc., 1992.

[9] F. Asano and Z.W. Luo, "Dynamic analyses of underactuated virtual passive dynamic walking," *Proc. of the IEEE Int. Conf. on Robotics and Automation*, pp. 3210–3217, 2007.

[10] F. Asano and Z.W. Luo, "The effect of semicircular feet on energy dissipation by heel-strike in dynamic bipedal walking," *Proc. of the IEEE Int. Conf. on Robotics and Automation*, pp. 3976–3981, 2007.

[11] A. Sano and J. Furusho, "Realization of natural dynamic walking using the angular momentum information," *Proc. of the IEEE Int. Conf. on Robotics and Automation*, pp. 1476–1481, 1990.